

# Grounded Human-Object Interaction Hotspots from Video

Tushar Nagarajan\*  
 UT Austin  
 tushar@cs.utexas.edu

Christoph Feichtenhofer  
 Facebook AI Research  
 feichtenhofer@fb.com

Kristen Grauman  
 Facebook AI Research  
 grauman@fb.com<sup>†</sup>

## Abstract

*Learning how to interact with objects is an important step towards embodied visual intelligence, but existing techniques suffer from heavy supervision or sensing requirements. We propose an approach to learn human-object interaction “hotspots” directly from video. Rather than treat affordances as a manually supervised semantic segmentation task, our approach learns about interactions by watching videos of real human behavior and recognizing afforded actions. Given a novel image or video, our model infers a spatial hotspot map indicating how an object would be manipulated in a potential interaction—even if the object is currently at rest. Through results with both first and third person video, we show the value of grounding affordance maps in real human-object interactions. Not only are our weakly supervised grounded hotspots competitive with strongly supervised affordance methods, but they can also anticipate object function for novel objects and enhance object recognition. Project page: <http://vision.cs.utexas.edu/projects/interaction-hotspots/>*

## 1. Introduction

Today’s visual recognition systems know how objects *look*, but not how they *work*. Understanding how objects function is fundamental to moving beyond passive perceptual systems (e.g., those trained for image recognition) to active, embodied agents that are capable of both perceiving and interacting with their environment—whether to clear debris in a search and rescue operation, cook a meal in the kitchen, or even engage in a social event with people. Gibson’s theory of affordances [12] provides a way to reason about object function. It suggests that objects have “action possibilities” (e.g. a chair affords sitting, a broom affords cleaning), and has been studied extensively in computer vision and robotics in the context of action, scene, and object understanding [17].

\*Work done during internship at Facebook AI Research.

<sup>†</sup>On leave from UT Austin (grauman@cs.utexas.edu).

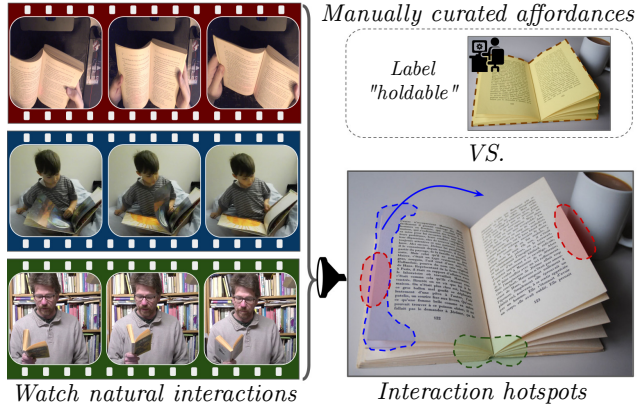


**Figure 1: Main idea.** Top right: Affordance labels given by human annotators capture expectations of what is important, which is often inconsistent with real interaction—technically, the entire book is “holdable”, but that does not reveal *how* books can be held. Left and bottom right: We propose to learn this *directly* from videos of people naturally interacting with objects, learning a representation that is grounded in real human behavior.

However, the abstract notion of “what actions are possible?” is only half the story. For example, for an agent tasked with sweeping the floor with a broom, knowing that the broom handle *affords holding* and the broom *affords sweeping* is not enough. The agent also needs to know *how* to interact with different objects, including the best way to grasp the object, the specific points on the object that need to be manipulated for a successful interaction, and how the object is used to achieve a goal.

Learning how to interact with objects is challenging. Traditional methods face two key limitations. First, methods that consider affordances as properties of an object’s shape or appearance [29, 13, 19] fall short of modeling actual object use and manipulation. In particular, learning to segment specified object parts [30, 38, 29, 31] can capture annotators’ expectations of what is important, but is detached from real interactions, which are dynamic, multi-modal, and may only partially overlap with part regions (see Figure 1). Secondly, existing methods are limited by their heavy supervision and/or sensor requirements. They as-

sume access to training images with manually drawn masks or keypoints [35, 9, 10] and some leverage additional sensors like depth [25, 48, 49] or force gloves [3], all of which restrict scalability. Such bottlenecks also deter generalization: exemplars are often captured in artificial lab tabletop environments [29, 25, 38] and labeling cost naturally restricts the scope to a narrow set of objects.

In light of these issues, we propose to learn affordances that are *grounded* in real human behavior directly from videos of people naturally interacting with objects, and without any keypoint or mask supervision. Specifically, we introduce an approach to infer an object’s *interaction hotspots*—the spatial or spatio-temporal regions most relevant to human-object interactions. Interaction hotspots link objects not only to the actions they afford, but also to *how* they afford them. By learning hotspots directly from video, we sidestep issues stemming from manual annotations, avoid imposing part labels detached from real interactions, and discover exactly how people interact with objects in the wild.

Our approach works as follows. We use videos of people performing everyday activities to learn an action recognition model. We show how to adapt our model to produce activations that are high-resolution, spatially localized, and predictive of human-object interaction. We derive interaction hotspots from these activations using class activation mapping [46, 39]. Then, we distill the information learned from video into a model for static images. Given a new image, we can hypothesize interaction hotspots for an object, even if it is not being actively manipulated.

We validate our model on two diverse video datasets: OPRA [10] and EPIC-Kitchens [6], spanning hundreds of object and action categories, with videos from both first and third person viewpoints. Our results show that with just weak action and object labels for video clips, our interaction hotspots can predict object affordances more accurately than other weakly supervised approaches, with relative improvements up to 22%. Furthermore, we show that our hotspot maps can anticipate object function for novel object classes that are never seen during training. Finally, we show that our learned features have impact beyond action understanding. By encoding objects not merely by their appearance, but also by their function, our approach benefits object recognition—even when objects are not being actively manipulated, as we demonstrate on MS COCO [28].

## 2. Related Work

**Visual Affordances.** The theory of affordances [12], originally from work in psychology, has been adopted to study several tasks in computer vision [17]. In action understanding, affordances provide context for action anticipation [26, 34, 47] and help learn stronger action recogni-

tion models [24]. In scene understanding, they help decide *where* in a scene a particular action can be performed [36, 13, 42, 8], learn scene geometry [16, 11], or understand social situations [5]. In object understanding, affordances help model object function and interaction [40, 43, 49, 14]. The choice of affordance representation varies significantly in these tasks, spanning across human pose, trajectories of objects, sensorimotor grasps, and 3D scene reconstructions. We focus on automatically learning appropriate representations for visual affordances from human-object interactions in video.

**Grounded Affordances.** Pixel-level segmentation of object parts [38, 29, 31] is a common affordance representation, for which supervised semantic segmentation frameworks are the typical approach [29, 35, 31, 9]. These segmentations convey high-level information about object function, but rely on manual mask annotations to train—which are not only costly, but can also give an unrealistic view of how objects are actually used. Unlike our approach, such methods are “ungrounded” in the sense that the annotator declares regions of interest on the objects outside of any interaction context.

Representations that are *grounded* in human behavior have also been explored. In images, human body pose serves as a proxy for object affordance to reveal modes of interaction with musical instruments [43, 44] or likely object interaction regions [4]. Given a video, methods can parse 3D models to estimate physical concepts (velocity, force, etc.) in order to categorize object interactions [48, 49]. For instructional video, methods explore ways to extract object states [1], modes of object interaction [7], interaction regions [10], or the anticipated trajectory of an object given a person’s skeleton pose [25].

We introduce a new approach for learning affordance “heatmaps” grounded in human-object interaction, as derived directly from watching real-world videos of people using the objects. Our model differs from other approaches in two main ways. First, no prior about interaction in the form of human pose, hand position, or 3D object reconstruction is used. All information about the interactions is learned directly from video. Second, rather than learn from manually annotated ground truth masks or keypoints [29, 35, 31, 9, 38, 37, 10], our model uses only coarse action labels for video clips to guide learning.

**Affordances for Object Understanding.** While cognitive science suggests that object affordance understanding may enhance humans’ ability to recognize objects [22], only limited prior work leverages affordances as context to improve object recognition. These include hand configuration [23], hand motion [41], sensorimotor grasp data [3], and object motion [14, 15]. In a similar spirit, we investigate how our representation learned from video can help object recognition. Specifically, given a novel image, we augment an ob-

ject’s observed visual features with hallucinated modes of interaction to facilitate recognition. Unlike prior methods, we rely only on RGB videos during training and we test on diverse, in-the-wild data that is not restricted to a lab setting.

### 3. Approach

Our goal is to learn “interaction hotspots”—characteristic spatio-temporal regions on objects that anticipate and explain human-object interactions (see Figure 1). Conventional approaches for learning affordance segmentation only address part of this goal. Their manually annotated segmentations are expensive to obtain, do not capture the dynamics of object interaction, and are based on the annotators’ notion of importance, which does not always align with real object interactions. Instead of relying on such segmentations as proxies for interaction, we train our model on a more direct source—videos of people naturally interacting with objects. We contend that such videos contain much of the cues necessary to piece together *how* objects are interacted with.

Our approach works as follows. First, we train a video action classifier to recognize each of the afforded actions (Section 3.1). Then, we adapt the resulting model to discover interaction hotspots on objects, without any keypoint or segmentation supervision (Section 3.2). Finally, given a static image of a novel object, we use the learned model to extract *hypotheses* of hotspots for various interactions (Section 3.3). Critically, the model can infer hotspots even for objects unseen during training and regardless of whether the object is actively being interacted with in the test image.

#### 3.1. Learning Afforded Actions from Video

Our key insight is to learn about object interactions from video. In particular, our approach learns to predict afforded actions across a span of objects, then recovers the object regions and object motions responsible for detecting each action. In this way, without explicit region labels and without direct estimation of physical contact points, we learn to anticipate object use.

Let  $\mathcal{A}$  denote the set of all afforded actions (e.g., *pourable*, *pushable*, *cuttable*), and let  $\mathcal{O}$  denote the set of object categories (e.g., *pan*, *chair*, *blender*), each of which affords one or more actions in  $\mathcal{A}$ . During training, we have video clips containing various combinations of afforded actions and objects.

First we train a video-classification model to predict which afforded action occurs in a video clip. For a video of  $T$  frames  $\mathcal{V} = \{f_1, \dots, f_T\}$ , we encode each frame using a convolutional neural network backbone to yield  $\{x_1, \dots, x_T\}$ . Each  $x_t$  is a tensor with  $d$  channels, each with  $n \times n$  spatial extent, with  $d$  and  $n$  determined by the specific

backbone used<sup>1</sup>. These features are then spatially pooled to obtain a  $d$ -dimensional vector per frame:

$$h_t(x_t) = P(x_t) \quad \text{for } t = 1, \dots, T, \quad (1)$$

where  $P$  denotes the pooling operator, to be specified below. We further aggregate all the frame-level features over time,

$$h_*(\mathcal{V}) = \mathbb{A}(h_1, \dots, h_T), \quad (2)$$

where  $\mathbb{A}$  is a *video aggregation module* that combines the frame features of a video into an aggregate feature  $h_*$  for the whole video. In our experiments, we use a long short-term memory (LSTM) recurrent neural network [20] for  $\mathbb{A}$ . We note that our framework is general and any video classification architecture (e.g. 3D ConvNets) can be used.

The aggregate video feature  $h_*$  is then fed to a linear classifier to predict the afforded action, which is trained using cross-entropy loss  $\mathcal{L}_{cls}$ . Once trained, this model can predict which action classes are observed in a video clip of arbitrary length. See Figure 2 (left) for the architecture.

Note that the classifier’s predictions are *object category-agnostic*, since we train it to recognize an afforded action across instances of any object category that affords that action. In other words, the classifier knows  $|\mathcal{A}|$  total actions, not  $|\mathcal{A}| \times |\mathcal{O}|$ ; it recognizes *pourable + X* as one entity, as opposed to *pourable + cup* and *pourable + bowl* separately. This point is especially relevant once we leverage the model below to generalize hotspots to unfamiliar objects.

#### 3.2. Generating Interaction Hotspot Maps

At test time, given frames  $\mathcal{Q} = \{q_1, \dots, q_T\}$ , our goal is to infer the *interaction hotspot* map  $\mathcal{H}_a$ , which is an  $H \times W$  matrix for each frame, summarizing the regions of interest that characterize an object interaction, for all  $a \in \mathcal{A}$ , where  $H, W$  denote the height and width of the source frame. Intuitively, a hotspot map should pick up on the regions of the object that would be manipulated during the action, indicative of its affordances, as well as the dynamic visual changes the object would exhibit during an interaction. Note that if  $T = 1$ , the novel input is simply a static image.

We devise an activation mapping [46] approach to go from interaction predictions to hotspots, tailoring it for discovering our hotspot maps. We start by defining a vanilla Grad-CAM technique, then explain our refinements. Grad-CAM [39] computes weighted linear combinations of intermediate convolutional neural network (CNN) activations to visualize the class-specific responses of a network. In our setting, the weights in this linear combination are derived from the gradients for the specific action  $a$ :

$$\alpha_k^a = \frac{1}{n^2} \sum_i \sum_j \frac{\partial y^a}{\partial x_{ij}^k}, \quad (3)$$

<sup>1</sup>For example, in our experiments using a modified ResNet [18] backbone, this results in  $d = 2048$  and  $n = 28$ , or a  $(2048, 28, 28)$ -dimension feature for each frame

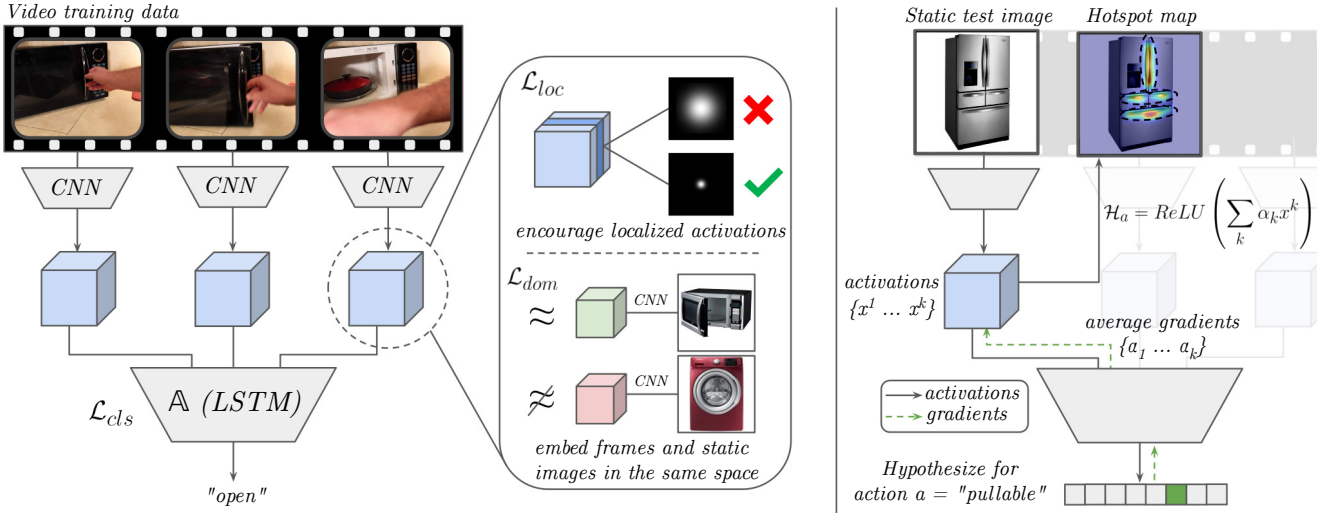


**Figure 2: Illustration of proposed framework.** The three components of our model (left panel)—the video action classifier (Section 3.1), the localized activation loss (Section 3.2), and the domain adaptation module (Section 3.2)—are jointly trained to predict the action class in a video clip, while implicitly building an affordance-aware internal representation for objects. Once trained (right panel), our model can generate “interaction hotspot” maps for a novel static input image as a linear combination of the learned interaction features, weighted by the gradients from a specific action. Our method can infer hotspots even for novel object categories unseen in the training video; for example, learning about opening microwaves helps anticipate how to open the fridge. Best viewed in color.

where  $x_{ij}^k$  refers to the  $(i, j)$  spatial activation value in the  $k^{th}$  channel of the input frame embedding. The normalized double summation refers to an average pooling operation. The preliminary hotspot map

$$\mathcal{H}_a(x) = \text{ReLU} \left( \sum_k \alpha_k^a x^k \right) \quad (4)$$

uses the weights as a form of spatial attention over the activations that positively influence the target afforded action. Using this, we discover important regions for a particular action, for each frame in the video, which serve as a coarse approximation of per-frame affordances.

The features learned in the vanilla model perform well for classification, but are insufficient for interaction hotspots due to their low spatial resolution and their diffused, global responses. We introduce several targeted modifications to address these issues, as follows.

**Localized Activations.** First, we address the spatial resolution. The reduced spatial resolution from repeatedly down-sampling features in the typical ResNet backbone is reasonable for classification, but is a bottleneck for learning interaction hotspots. Thus we use dilated convolutions [45] and reduced strides in our final convolution layers to increase the final spatial resolution to  $n = 28$ , allowing our heatmaps to capture finer details.

Second, we adapt the network to encourage more localized activations. Inspired by [32], we use max-pooled features to identify the spatial locations that respond most

strongly to an afforded action. This corresponds to

$$h_t(x_t) = P_{max}(x_t), \quad \text{for } t = 1, \dots, T, \quad (5)$$

for Equation 1, where  $P_{max}$  denotes the max pooling operator. Unlike the uniform gradients produced by average-pooling, the gradients of the max operation are location selective, which helps learn more strongly localized features.

To account for the sparse gradients that occur from the max-pool operation, we introduce an auxiliary loss term  $\mathcal{L}_{loc}$  that uses average pooled features to penalize high activations for *only the negative classes*. For a video with frame embeddings  $\{x_1, \dots, x_T\}$  and true action  $a$  we compute:

$$g_t(x_t) = P_{avg}(x_t) \quad \text{for } t = 1, \dots, T \quad (6)$$

for its frames, and aggregate the results as

$$g_*(\mathcal{V}) = \mathbb{A}(g_1, \dots, g_T) \quad (7)$$

Then we define the auxiliary loss as:

$$\mathcal{L}_{loc}(\mathcal{V}, a) = \sum_{a' \in \mathcal{A} \setminus \{a\}} [\sigma(W^T g_* + b)]_{a'} \quad (8)$$

where  $\sigma(\cdot)$  is the sigmoid function,  $P_{avg}$  denotes average pooling, and  $(W, b)$  denotes the action classifier parameters. These two modifications encourage activations for *correct* afforded actions to be more localized, while forcing uniformly low spatial activations for *incorrect* actions.

**Domain Adaptation.** We aim for our system to learn about object affordances by watching first-person video of people handling objects, then map that knowledge to third-person web photos. For this, our model trained on videos needs to be able to process static images that have considerably different viewpoint and scale.

To bridge this *domain gap* between videos and static images, we introduce a triplet loss term that encourages frames of a video  $\mathcal{V}$  containing an object  $o \in \mathcal{O}$  to be similar to a static image  $\mathcal{I}_o$  of the same object, and different from a static image of a different object class  $\mathcal{I}_{o'}$ ,  $o' \neq o$ . The domain adaptation loss is:

$$\mathcal{L}_{dom}(\mathcal{V}, \mathcal{I}_o, \mathcal{I}_{o'}) = \max [0, d(h_*(x_i), h_*(x_o)) - d(h_*(x_i), h_*(x_{o'})) + M], \quad (9)$$

where  $x_i$  is the image embedding of a randomly selected frame from  $\mathcal{V}$ ,  $x_o$  and  $x_{o'}$  are image embeddings of  $\mathcal{I}_o$  and  $\mathcal{I}_{o'}$ , respectively,  $d$  denotes Euclidean distance, and  $M$  is the margin value, which we keep fixed at 0.5 for our experiments. Note that the model treats these images as single-frame videos. This term forces our model to treat frames from videos and static images the same way, resulting in a robust model that can be used for both.

### 3.3. Training and Inference

During training, we generate embeddings  $\{x_1, \dots, x_T\}$  for each frame of a video. These frames are passed through  $\mathbb{A}$  to generate the video embedding  $h_*$ , and finally through a classifier to predict the afforded action label. The complete loss function applied to each training video  $\mathcal{V}$  is:

$$\mathcal{L}(\mathcal{V}, a) = \mathcal{L}_{cls}(\mathcal{V}, a) + \mathcal{L}_{loc}(\mathcal{V}, a) + \mathcal{L}_{dom}(\mathcal{V}, \mathcal{I}_o, \mathcal{I}_{o'}). \quad (10)$$

For inference on a static image, we first generate its image embedding  $x$ . Then, we predict potential afforded actions, by treating this image as a single frame video. Finally, using Equation 4 we generate  $|\mathcal{A}|$  heatmaps, one for each afforded action class. This stack of heatmaps are the *interaction hotspots*. Our model can similarly produce hotspots for input videos, when available, by using all  $T$  frames to generate the aggregated video representation  $h_*$ .

We stress that the interaction hotspots are predictable even for unfamiliar objects. By training the afforded actions across object category boundaries, the system learns the general properties of appearance *and* interaction that characterize affordances. Hence, our approach can anticipate, for example, how an unfamiliar kitchen device might be used because it has learned how a variety of other objects operate. Similarly, heatmaps can be hallucinated for novel action-object pairs (*e.g.* “cut” using a spatula in Figure 5, last column) that have not been seen in training.

	Supervision Source	Type	$N$
GAZE [21]	Recorded eye fixations	Weak	60k
SALIENCY [33]	Manual saliency labels	Weak	10k
OURS	Action, object labels	Weak	20k
IMG2HEATMAP	Manual affordance keypoints	Strong	20k
DEMO2VEC [10]	Manual affordance keypoints, action labels	Strong	20k

**Table 1: Supervision source and type for all methods.** Our method learns interaction hotspots *without* strong supervision like annotated segmentation/keypoints.  $N$  is the number of instances.

## 4. Experiments

Our experiments on interaction hotspots explore their ability to describe affordances of objects, to generalize to anticipate affordances of unfamiliar objects, and to aid object recognition.

### 4.1. Experimental setup

**Datasets.** We use three datasets:

- **OPRA** [10] contains videos of product reviews of common appliances (*e.g.* refrigerators, coffee machines) collected from YouTube. Each instance is a short video demonstration  $\mathcal{V}$  of a product’s feature (*e.g.* pressing a button on a coffee machine) paired with a static image  $\mathcal{I}$  of the product, an interaction label  $a$  (*e.g.* “pressing”), and a manually created affordance heatmap  $\mathcal{M}$  (*e.g.* highlighting the button on the static image). There are  $\sim 16k$  training instances of the form  $(\mathcal{V}, \mathcal{I}, a, \mathcal{M})$ , spanning 7 actions.
- **EPIC-Kitchens** [6] contains unscripted, egocentric videos of activities in a kitchen. Each clip  $\mathcal{V}$  is annotated with action and object labels  $a$  and  $o$  (*e.g.* cut tomato, open refrigerator) along with a set of bounding boxes  $\mathcal{B}$  (one per frame) for objects being interacted with. There are  $\sim 40k$  training instances of the form  $(\mathcal{V}, a, o, \mathcal{B})$ , spanning 352 objects and 125 actions.
- **COCO** [28] is a popular object detection benchmark containing static images and bounding boxes around 80 object categories. We take all 20 object classes that overlap with those in EPIC-Kitchens to create an object recognition testbed (cf. Sec 4.3).

The two video datasets span diverse settings. OPRA has third person videos, where the person and the product being reviewed are clearly visible, and covers a small number of actions and products. EPIC-Kitchens has first-person videos of unscripted kitchen activities and a much larger vocabulary of actions and objects; the person is only partially visible when they manipulate an object. Together, they pro-

	KLD $\downarrow$	SIM $\uparrow$	CC $\uparrow$	AUC-J $\uparrow$	NSS $\uparrow$	Acc (%)
WS	CENTER BIAS	4.21	0.18	0.10	0.58	0.30
	GAZE [21]	2.79	0.18	0.07	0.62	0.25
	SALIENCY [33]	2.09	0.25	0.20	<b>0.74</b>	0.73
	OURS	<b>1.76</b>	<b>0.26</b>	<b>0.24</b>	<b>0.74</b>	<b>0.86</b>
SS	IMG2HEATMAP	1.69	0.29	0.28	0.80	1.20
	DEMO2VEC [10]	<b>1.44</b>	<b>0.35</b>	<b>0.38</b>	<b>0.84</b>	<b>1.62</b>
						49.4
						40.8

**Table 2: Grounded affordance prediction** Our model outperforms other weakly supervised (WS) methods in all metrics, and scores within 4%-28% of strongly supervised (SS) methods *without* the privilege of heatmap annotations during training.  $\uparrow/\downarrow$  indicates higher/lower is better.

vide good variety and difficulty to evaluate the robustness of our model.<sup>2</sup>

For both datasets, our model uses only the action labels as supervision, and object labels to select static images for our domain adaptation loss  $\mathcal{L}_{dom}$  (details in Supp.). The annotated heatmap  $\mathcal{M}$  is used only for evaluation.

**Implementation Details.** For all experiments, we use an ImageNet [27] pretrained ResNet-50 [18] modified for higher output resolution. To increase the output dimension from  $n = 7$  to  $n = 28$ , we set the spatial stride of  $res_4$  and  $res_5$  to 1 (instead of 2), and use dilation of 2 ( $res_4$ ) and 4 ( $res_5$ ) for its filters to preserve the original scale. The  $res_5$  block is followed by a randomly initialized convolutional layer ( $d = 2048$ ). We use a single layer LSTM (hidden size 2048) as  $\mathbb{A}$ , and a maximum temporal length of 32 frames per video during training. More details are in Supp.

## 4.2. Interaction Hotspots as Grounded Affordances

In this section, we evaluate two things: 1) How well does our model implicitly learn object affordances? and 2) How well can it infer possible interactions for unfamiliar objects? For this, we train our model on video clips, and generate hotspot maps on *static images*.

**Baselines.** We evaluate our model against several baselines and state-of-the-art models.

- **CENTER BIAS** produces a fixed Gaussian heatmap at the center of the image. This is a naive baseline to account for a possible center bias.
- **SALIENCY** [33] estimates the most salient regions in an image. We use the authors’ pretrained model.
- **GAZE** [21] is a gaze prediction model trained on ego-centric video. We use the authors’ pretrained model, omitting the flow stream since inputs are static images.
- **DEMO2VEC** [10] is a supervised method that generates an affordance heatmap using context from a video

<sup>2</sup>Other affordance segmentation datasets [29, 30] have minimal overlap with the OPRA and EPIC-Kitchens classes, and hence do not permit evaluation for our setting, since we learn from video.



**Figure 3: Generated affordance heatmaps on static images.** Left: Predicted affordance heatmaps for 3 actions (hold, rotate, push), shown as red, green, and blue regions on static images from OPRA. Our model highlights unique spatial affordances consistent with how people interact with the objects. Note that SALIENCY produces only a single “importance” heatmap (yellow). Last column shows a failure case. (Best viewed in color)

demonstration of the interaction. We use the authors’ pre-computed heatmap predictions.

- **IMG2HEATMAP** is a supervised method that uses a fully convolutional encoder-decoder to predict the affordance heatmap for an image. It serves as a simplified version of DEMO2VEC that lacks video context during training.

SALIENCY and GAZE capture a generic notion of spatial *importance*. They produce a single heatmap for an image, regardless of action class, and as such, are less expressive than per-action-affordances. They are *weakly supervised* in that they are trained for a different task, albeit with strong supervision (heatmaps, gaze points) for that task. DEMO2VEC and IMG2HEATMAP are strongly supervised, and represent more traditional affordance learning techniques that learn affordances from manually labeled images [29, 35, 31, 9]. Table 1 summarizes the sources and types of supervision for all methods. Unlike other methods, our model uses only weak class labels during training.

**Grounded Affordance Prediction.** First we compare the ground truth OPRA heatmaps for each interaction to our hotspots and the baselines’ heatmaps. We report error as KL-Divergence, following [10], as well as several metrics (AUC-J, NSS, SIM, CC) from the saliency literature [2].

Table 2 summarizes the results. Our model outperforms all other weakly-supervised methods in all metrics, with relative improvements of up to 22% (in CC) compared to the strongest baseline. These results highlight that our model can capture sophisticated interaction cues that describe more specialized notions of importance than saliency.

GAZE is trained on gaze fixation points that are predictive of coarse object location, but need not correlate

	KLD $\downarrow$	SIM $\uparrow$	CC $\uparrow$	AUC-J $\uparrow$	NSS $\uparrow$
CENTER BIAS	3.26	0.21	0.03	0.56	0.09
GAZE [21]	1.70	0.35	0.02	0.54	0.03
SALIENCY [33]	1.29	0.44	0.08	0.61	0.23
OURS	0.65	<b>0.66</b>	<b>0.69</b>	<b>0.94</b>	<b>2.45</b>
IMG2HEATMAP	<b>0.45</b>	0.61	0.21	0.71	0.59

**Table 3: Generalization to novel objects.** Our model can accurately reconstruct the interaction hotspots for object *categories* that were unseen during training, highlighting its ability to generalize on an object-function level.

well with object affordances. SALIENCY performs slightly worse than our model, though it may accidentally benefit from the fact that OPRA’s kitchen appliances have interaction regions (*e.g.* buttons, handles) designed to be visually salient. In contrast to our approach, neither GAZE nor SALIENCY distinguish between affordances; they produce a single heatmap representing “important” salient points. To these methods, the blade of a knife is as important to the action “cutting” as it is to the action “holding”, limiting their ability to explain objects with multiple affordances.

IMG2HEATMAP and DEMO2VEC generate better affordance heatmaps, but at the cost of strong supervision. Compared to both baselines, our method produces affordance heatmaps without manual heatmaps as supervision for training. Also, it does so without sacrificing action recognition accuracy. We achieve significantly better results on the OPRA test set (49.4% vs. 40.8% reported in [10]), suggesting the multi-task model in [10] gives up some representational power by explicitly addressing both tasks.

Ablation experiments isolating the model enhancements we introduced in Sec 3.2 reveal that they are valuable to accurately capture affordances. Please see Supp.

Figure 3 shows example heatmaps generated by our method for static images from OPRA, compared to other methods. Our model is able to highlight specific object regions that afford actions (*e.g.* the handblender handle as “holdable” in column 1) after only watching videos of object interactions. Weakly supervised methods like GAZE and SALIENCY tend to highlight *all* salient object parts in a single heatmap, regardless of the interaction in question. Our model is specific, and can highlight multiple distinct affordances for an object. To generate comparable heatmaps, DEMO2VEC requires annotated heatmaps for training *and* a set of video demonstrations during inference, while our model can hypothesize object functionality without these extra requirements.

**Generalization to Novel Objects** Can interaction hotspots infer how novel object categories work? We next test if our model learns an *object-agnostic* representation for interaction—one that is not tied to object class. This is a useful property for open-world situations where unfamiliar



**Figure 4: Interaction hotspots on EPIC-Kitchens videos.** When applied to video, our model highlights spatial interaction regions (*e.g.* door handles, knife blades) as well as temporal signatures (*e.g.* swinging of doors). Critically, the object categories shown in this figure have *not* been seen during training; our model learns to generalize interaction hotspots. For example, there are no fridges or drawers in the training video, but our method anticipates how these objects would be opened.

objects may have to be interacted with to achieve a goal.

We divide the object categories  $\mathcal{O}$  into familiar and unfamiliar object categories  $\mathcal{O} = \mathcal{O}_f \cup \mathcal{O}_u$ ; familiar ones are those seen with interactions in training video and unfamiliar ones are seen only during testing. We divide our video train/test sets along these object splits, making sure that the number of training videos for both sets is approximately equal. We perform this experiment on EPIC Kitchens since it has the object labels needed to form the data splits.

We train two models: OURS-ALL trained on all clips, with any objects from  $\mathcal{O}$ , and OURS-FAMILIAR trained only on clips with the familiar objects from  $\mathcal{O}_f$ . We generate interaction hotspot maps using OURS-ALL on the held out clips with unfamiliar objects from  $\mathcal{O}_u$ . These “oracle” maps represent how novel objects *would have* been interacted with. If OURS-FAMILIAR can successfully reconstruct them, it implies that a general sense of object function is learned that is not strongly tied to object identity.

Table 3 shows the results. Our model is able to recover the hotspot maps for unfamiliar objects substantially better than other methods. Compared to Table 2, we can see that the interaction agnostic methods are not able to reconstruct the maps very well. This may be due to two factors. First, the held-out heatmaps are predictions from our model,

N →	EPIC Kitchens				COCO			
	5	25	100	280 (all)	5	25	100	3300 (all)
RESNET	5.9 ± 0.1	16.0 ± 0.2	24.5 ± 0.5	<b>26.5 ± 0.1</b>	44.3 ± 0.3	56.6 ± 0.2	<b>65.6 ± 0.4</b>	<b>75.2 ± 0.1</b>
AUTOENCODER	4.9 ± 0.2	12.8 ± 0.1	21.9 ± 0.2	23.9 ± 0.3	39.4 ± 0.4	51.2 ± 0.2	59.1 ± 0.2	72.8 ± 0.3
OURS	<b>7.9 ± 0.2</b>	<b>16.7 ± 0.2</b>	<b>25.0 ± 0.2</b>	26.0 ± 0.2	<b>46.8 ± 0.3</b>	<b>57.9 ± 0.1</b>	63.2 ± 0.2	73.9 ± 0.3

**Table 4: Low-shot object recognition accuracy (%)** Our model learns interaction features that help object recognition in low shot settings ( $N < 100$ ) where appearance information alone is insufficient. We report average classification accuracy and standard error over 20 runs.



**Figure 5: Low-shot object recognition on EPIC and COCO.** Qualitative examples of interaction hotspot maps on EPIC and COCO for actions cut, mix, hold and open (red, green, blue, cyan) are shown below the table. Best viewed electronically.

rather than annotated ground truth. Though the categories are unseen by all methods, using the same model architecture may allow us to inherit some biases that give us a slight edge for reproducing heatmaps. More importantly, the evaluation is performed across a much larger set of action classes, which demands more diverse, interaction-specific maps. Models that generate a fixed saliency heatmap do not perform well in this situation. Note that DEMO2VEC is not applicable here as predictions on EPIC-Kitchens is not available.

Qualitative results (Figure 4) support our numbers, showing our model applied directly to video clips from EPIC Kitchens. Our model—which was never trained on some objects (*e.g.* fridges, drawers)—captures both the spatial location (*e.g.* door/drawer handles) as well as the characteristic dynamics (*e.g.* swinging refrigerator door) of interactions.

### 4.3. Interaction Hotspots for Object Recognition

Finally, inspired by cognitive science findings [22], we test the idea that interaction hotspots provide cues for identifying objects (*e.g.* objects that swing open are *door-like*) in scenarios where appearance based features are insufficient.

We consider object recognition tasks on two datasets, EPIC-Kitchens and COCO [28], composed of 352 and 20 object classes, respectively. See Supp. for data setup details. We use our model trained on EPIC videos to *hallucinate* modes of interaction for novel objects in COCO via

hotspots, which are then fed as a separate input stream to an object classifier. We vary the number of training examples per class ( $N$ ) in order to study our model’s contributions under different levels of supervision. Further, we introduce a baseline AUTOENCODER, which learns a compact representation over all training video, to make sure any gains by our method are not simply due to having seen more video during training. Model architecture details are in Supp.

Table 4 shows our results. Using interaction features from our model consistently improves object recognition in low shot settings by  $\sim 2\%$  on both datasets, while matching the performance when trained on all data. The compressed representation produced by AUTOENCODER provides redundant information to the object classifier, leading to overfitting when  $N$  is small. We believe this is an especially encouraging result for hotspots: the model has never seen images from COCO during training, yet it can generate useful interaction features that improve object recognition.

## 5. Conclusion

We presented a method to learn “interaction hotspot” maps—characteristic spatio-temporal regions over objects that anticipate and explain object interactions, directly from watching videos of people naturally interacting with objects. Our experiments show that these hotspot maps explain object affordances better than other existing weakly supervised models and can generalize to anticipate affordances of unseen objects as well. In addition, our model

provides useful *object function* cues that improve object recognition on static images. In future work, we plan to explore how these representations can be useful for action anticipation, and how to extend them for embodied robot agents to help learn better policies for object interaction.

**Acknowledgments:** We would like to thank the authors of Demo2Vec [10] for their help with the OPRA dataset. We would also like to thank Marcus Rohrbach and Jitendra Malik for the helpful discussions.

## References

- [1] J.-B. Alayrac, J. Sivic, I. Laptev, and S. Lacoste-Julien. Joint discovery of object states and manipulation actions. *ICCV*, 2017. [2](#)
- [2] Z. Bylinskii, T. Judd, A. Oliva, A. Torralba, and F. Durand. What do different evaluation metrics tell us about saliency models? *TPAMI*, 2018. [6](#)
- [3] C. Castellini, T. Tommasi, N. Noceti, F. Odone, and B. Caputo. Using object affordances to improve object recognition. *TAMD*, 2011. [2](#)
- [4] C.-Y. Chen and K. Grauman. Subjects and their objects: Localizing interactees for a person-centric view of importance. *IJCV*, 2016. [2](#)
- [5] C.-Y. Chuang, J. Li, A. Torralba, and S. Fidler. Learning to act properly: Predicting and explaining affordances from images. *CVPR*, 2018. [2](#)
- [6] D. Damen, H. Doughty, G. M. Farinella, S. Fidler, A. Furnari, E. Kazakos, D. Moltisanti, J. Munro, T. Perrett, W. Price, et al. Scaling egocentric vision: The epic-kitchens dataset. *ECCV*, 2018. [2, 5](#)
- [7] D. Damen, T. Leelasawassuk, O. Haines, A. Calway, and W. W. Mayol-Cuevas. You-do, i-learn: Discovering task relevant objects and their modes of interaction from multi-user egocentric video. In *BMVC*, 2014. [2](#)
- [8] V. Delaitre, D. F. Fouhey, I. Laptev, J. Sivic, A. Gupta, and A. A. Efros. Scene semantics from long-term observation of people. In *ECCV*, 2012. [2](#)
- [9] T.-T. Do, A. Nguyen, I. Reid, D. G. Caldwell, and N. G. Tsagarakis. Affordancenet: An end-to-end deep learning approach for object affordance detection. *ICRA*, 2017. [2, 6](#)
- [10] K. Fang, T.-L. Wu, D. Yang, S. Savarese, and J. J. Lim. Demo2vec: Reasoning object affordances from online videos. In *CVPR*, 2018. [2, 5, 6, 7, 9](#)
- [11] D. F. Fouhey, V. Delaitre, A. Gupta, A. A. Efros, I. Laptev, and J. Sivic. People watching: Human actions as a cue for single view geometry. *IJCV*, 2014. [2](#)
- [12] J. J. Gibson. *The ecological approach to visual perception: classic edition*. Psychology Press, 1979. [1, 2](#)
- [13] H. Grabner, J. Gall, and L. Van Gool. What makes a chair a chair? In *CVPR*, 2011. [1, 2](#)
- [14] A. Gupta and L. S. Davis. Objects in action: An approach for combining action understanding and object perception. In *CVPR*, 2007. [2](#)
- [15] A. Gupta, A. Kembhavi, and L. S. Davis. Observing human-object interactions: Using spatial and functional compatibility for recognition. *TPAMI*, 2009. [2](#)
- [16] A. Gupta, S. Satkin, A. A. Efros, and M. Hebert. From 3d scene geometry to human workspace. In *CVPR*, 2011. [2](#)
- [17] M. Hassanin, S. Khan, and M. Tahtali. Visual affordance and function understanding: A survey. *arXiv preprint arXiv:1807.06775*, 2018. [1, 2](#)
- [18] K. He, X. Zhang, S. Ren, and J. Sun. Deep residual learning for image recognition. In *CVPR*, 2016. [3, 6](#)
- [19] T. Hermans, J. M. Rehg, and A. Bobick. Affordance prediction via learned object attributes. In *ICRA: Workshop on Semantic Perception, Mapping, and Exploration*, 2011. [1](#)
- [20] S. Hochreiter and J. Schmidhuber. Long short-term memory. *Neural computation*, 1997. [3](#)
- [21] Y. Huang, M. Cai, Z. Li, and Y. Sato. Predicting gaze in egocentric video by learning task-dependent attention transition. *ECCV*, 2018. [5, 6, 7](#)
- [22] J. Kilner, A. Neal, N. Weiskopf, K. Friston, and C. Frith. Evidence of mirror neurons in human inferior frontal gyrus. *Journal of Neuroscience*, 2009. [2, 8](#)
- [23] H. Kjellström, J. Romero, and D. Kragić. Visual object-action recognition: Inferring object affordances from human demonstration. *CVIU*, 2011. [2](#)
- [24] H. S. Koppula, R. Gupta, and A. Saxena. Learning human activities and object affordances from rgbd videos. *IJR*, 2013. [2](#)
- [25] H. S. Koppula and A. Saxena. Physically grounded spatio-temporal object affordances. In *ECCV*, 2014. [2](#)
- [26] H. S. Koppula and A. Saxena. Anticipating human activities using object affordances for reactive robotic response. *TPAMI*, 2016. [2](#)
- [27] A. Krizhevsky, I. Sutskever, and G. E. Hinton. Imagenet classification with deep convolutional neural networks. In *NIPS*, 2012. [6](#)
- [28] T.-Y. Lin, M. Maire, S. Belongie, J. Hays, P. Perona, D. Ramanan, P. Dollár, and C. L. Zitnick. Microsoft coco: Common objects in context. In *ECCV*, 2014. [2, 5, 8](#)
- [29] A. Myers, C. L. Teo, C. Fermüller, and Y. Aloimonos. Affordance detection of tool parts from geometric features. In *ICRA*, 2015. [1, 2, 6](#)
- [30] A. Nguyen, D. Kanoulas, D. G. Caldwell, and N. G. Tsagarakis. Detecting object affordances with convolutional neural networks. In *IROS*, 2016. [1, 6](#)
- [31] A. Nguyen, D. Kanoulas, D. G. Caldwell, and N. G. Tsagarakis. Object-based affordances detection with convolutional neural networks and dense conditional random fields. In *IROS*, 2017. [1, 2, 6](#)
- [32] D. Novotný, D. Larlus, and A. Vedaldi. Anchornet: A weakly supervised network to learn geometry-sensitive features for semantic matching. In *CVPR*, 2017. [4](#)
- [33] J. Pan, C. C. Ferrer, K. McGuinness, N. E. O'Connor, J. Torres, E. Sayrol, and X. Giro-i Nieto. Salgan: Visual saliency prediction with generative adversarial networks. *arXiv preprint arXiv:1701.01081*, 2017. [5, 6, 7](#)
- [34] N. Rhinehart and K. M. Kitani. Learning action maps of large environments via first-person vision. In *CVPR*, 2016. [2](#)
- [35] A. Roy and S. Todorovic. A multi-scale cnn for affordance segmentation in rgbd images. In *ECCV*, 2016. [2, 6](#)

- [36] M. Savva, A. X. Chang, P. Hanrahan, M. Fisher, and M. Nießner. Scenegrok: Inferring action maps in 3d environments. *TOG*, 2014. [2](#)
- [37] J. Sawatzky and J. Gall. Adaptive binarization for weakly supervised affordance segmentation. *ICCV: Workshop on Assistive Computer Vision and Robotics*, 2017. [2](#)
- [38] J. Sawatzky, A. Srikantha, and J. Gall. Weakly supervised affordance detection. In *CVPR*, 2017. [1](#), [2](#)
- [39] R. R. Selvaraju, M. Cogswell, A. Das, R. Vedantam, D. Parikh, D. Batra, et al. Grad-cam: Visual explanations from deep networks via gradient-based localization. In *ICCV*, 2017. [2](#), [3](#)
- [40] M. Stark, P. Lies, M. Zillich, J. Wyatt, and B. Schiele. Functional object class detection based on learned affordance cues. In *ICVS*, 2008. [2](#)
- [41] S. Thermos, G. T. Papadopoulos, P. Daras, and G. Potamianos. Deep affordance-grounded sensorimotor object recognition. *CVPR*, 2017. [2](#)
- [42] X. Wang, R. Girdhar, and A. Gupta. Binge watching: Scaling affordance learning from sitcoms. In *CVPR*, 2017. [2](#)
- [43] B. Yao and L. Fei-Fei. Grouplet: A structured image representation for recognizing human and object interactions. In *CVPR*, 2010. [2](#)
- [44] B. Yao, J. Ma, and L. Fei-Fei. Discovering object functionality. In *ICCV*, 2013. [2](#)
- [45] F. Yu and V. Koltun. Multi-scale context aggregation by dilated convolutions. *ICLR*, 2016. [4](#)
- [46] B. Zhou, A. Khosla, A. Lapedriza, A. Oliva, and A. Torralba. Learning deep features for discriminative localization. In *CVPR*, 2016. [2](#), [3](#)
- [47] Y. Zhou, B. Ni, R. Hong, X. Yang, and Q. Tian. Cascaded interactional targeting network for egocentric video analysis. In *CVPR*, 2016. [2](#)
- [48] Y. Zhu, C. Jiang, Y. Zhao, D. Terzopoulos, and S.-C. Zhu. Inferring forces and learning human utilities from videos. In *CVPR*, 2016. [2](#)
- [49] Y. Zhu, Y. Zhao, and S. Chun Zhu. Understanding tools: Task-oriented object modeling, learning and recognition. In *CVPR*, 2015. [2](#)

## 6. Supplementary Material

This section consists of supplementary material to support the main paper text. The contents include:

- Details about how the images ( $\mathcal{I}$  and  $\mathcal{I}'$ ) for the domain adaptation loss in Section 3.2 are selected
- Ablation experiments isolating the model enhancements introduced in Section 3.2
- Architecture details for the IMAGE2HEATMAP model introduced in Section 4.2 (Baselines)
- Additional details about the evaluation protocol for our experiments on the OPRA dataset in Section 4.2
- Additional training details including hyper-parameter selection for all experiments in Section 4.2
- Dataset and model details for the low shot object recognition experiments in Section 4.3
- More examples of hotspots generated on all three datasets to supplement Figure 3 and Figure 5 in the main paper.

### Selecting Images for the Domain Adaptation Loss $\mathcal{L}_{dom}$

The domain adaptation term presented in Section 3.2 of the main paper requires a positive and negative image ( $\mathcal{I}_o$  and  $\mathcal{I}_{o'}$ ) for the triplet loss. For OPRA instances of the form  $(\mathcal{V}, \mathcal{I}, a, \mathcal{M})$ , we use the static image  $\mathcal{I}$  paired with each video as the positive image, and the one from a different instance (of a different product) as the negative image in Equation 9. For EPIC-Kitchens instances of the form  $(\mathcal{V}, a, o, \mathcal{B})$ , we take the center frame of each clip, crop out the object being interacted with using the respective bounding box from  $\mathcal{B}$ , and treat that as our static image for the instance as before.

### Ablation Study: Effect of Affordance-aware Model Modifications

We report ablation experiments for our model enhancements presented in Section 3.2. Table 4 shows these results. Each row corresponds to adding one of our modifications to the standard ResNet-50 model. These include increased spatial resolution, our localization loss, and our domain adaptation term respectively. Each of the modifications results in an increase in our model’s capacity to represent object affordances. Increasing the spatial resolution from  $7 \times 7$  to  $28 \times 28$  using dilated convolutions results in a large increase in performance (up to 22% in some metrics). The localization and domain adaption losses on their own contribute a small increase in performance, but together, produce a dramatic increase across all metrics. Together, these modifications help make a standard recognition model *affordance-aware*, allowing it to implicitly build a representation for object interaction on the fly.

	KLD $\downarrow$	SIM $\uparrow$	CC $\uparrow$	AUC-J $\uparrow$	NSS $\uparrow$
BASE	2.34	0.18	0.13	0.58	0.35
+N=28	2.18	0.17	0.16	0.61	0.43
+ONLY LOC	2.91	0.15	0.10	0.57	0.32
+ONLY DOM	2.88	0.18	0.12	0.60	0.49
+LOC+DOM	<b>1.76</b>	<b>0.26</b>	<b>0.24</b>	<b>0.74</b>	<b>0.86</b>

**Table 4: Ablation study of model enhancements. Metrics as defined in the main text.**

### Architecture Details for Supervised Baselines

The IMAGE2HEATMAP model in Section 4.2 is a fully convolutional encoder-decoder to predict the affordance heatmap for an image. The encoder is an ImageNet pretrained VGG16 backbone (up to conv5), resulting in an encoded feature with 512 channels and spatial extent 7. This feature is passed through a decoder with an architecture mirroring the backbone, where the max-pooling operations are replaced with bilinear upsampling operations. This results in an output of the same dimension as the input, and as many channels as the number of actions. The output of this network is fed through a Sigmoid operator and reconstruction loss against the ground truth affordance heatmap is calculated using binary cross-entropy.

### Evaluation Protocol for Grounded Affordance Prediction

As discussed in Section 4.2, the heatmaps generated by our model and the baselines are evaluated against the manually annotated ground truth heatmaps provided in the OPRA dataset (results in Table 2 and Table 3). For a single action (e.g. “press” a button), the ground truth heatmaps may occur distributed across several instances (e.g. different clips of people

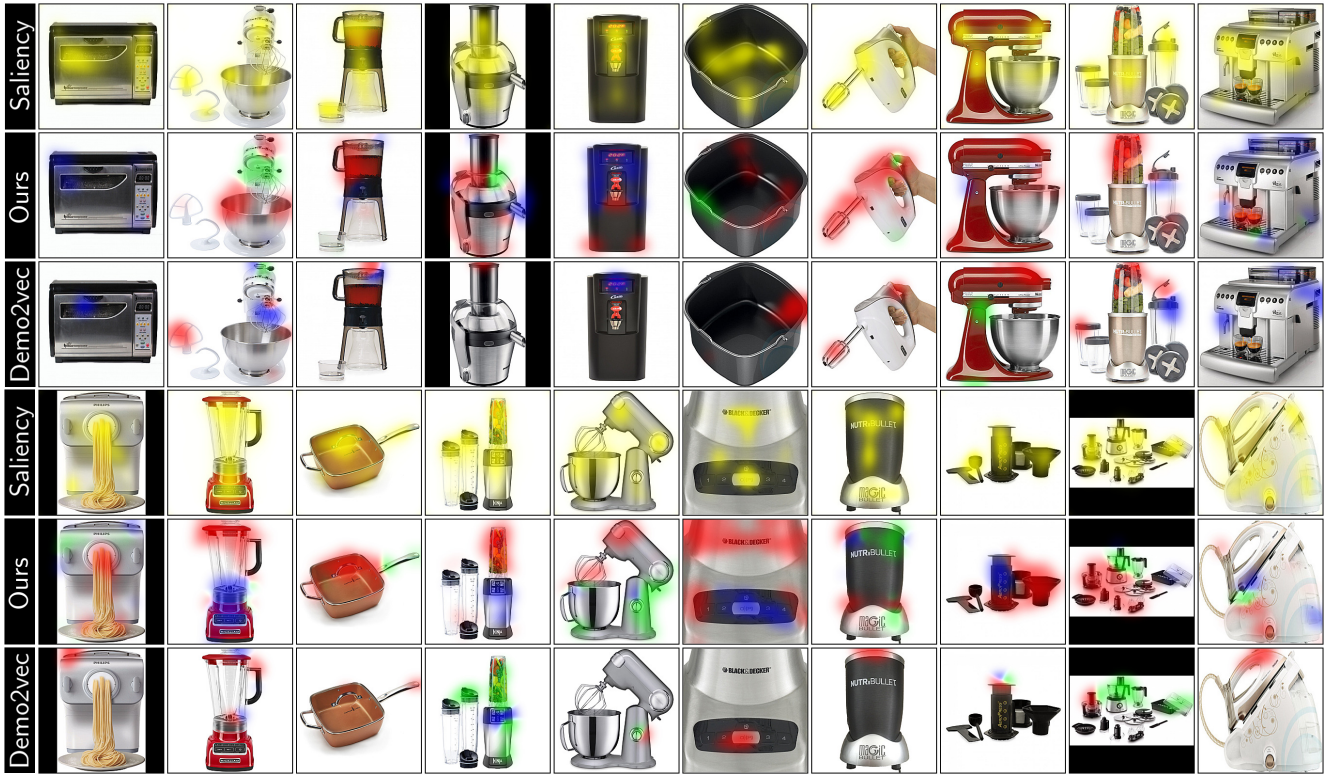


**Figure 6: Generated affordance heatmaps on static images from OPRA.** Our interaction hotspot maps show holdable, rotatable, and pushable regions (in red, green, and blue respectively). Saliency heatmaps do not discriminate between interactions and produce a single heatmap shown in yellow. Recall that the Demo2Vec approach (Fang et al.) is strongly supervised, whereas our approach is weakly supervised. Some failure cases due to small or unfamiliar objects can be seen in the last 4 examples.

pressing different buttons on the same object). We simply take the union of all these heatmaps as our target affordance heatmap for the action. This leaves us with  $\sim 1k$  (image, action pairs for evaluation) involving  $\sim 250$  unique objects (about 4 affordances per object on average). For AUC-J, we binarize heatmaps using a threshold of 0.5 for evaluation.

## Additional Training Details

We provide additional details to accompany Section 4.1 (Implementation Details) in the main paper. In our combined loss, we equally weight all three loss terms. As mentioned in Section 3.2 we keep the margin in our triplet loss term fixed at 0.5, thus we normalize the inputs before computing the triplet loss. Our models are implemented in PyTorch. SGD with momentum 0.9, learning rate 1e-3, weight decay 5e-4 and batch size 64 is used to optimize the models parameters.

## Low-shot Recognition Experimental Setup Details

We provide additional details about the dataset construction and the model architecture used for the experiments in Section 4.3 in the main paper. We construct an object-recognition split of EPIC-Kitchens and MS COCO as follows. For EPIC-Kitchens, we use the provided object bounding boxes to crop out the object from the center frame of each interaction clip, and compile these into our dataset for classification. For COCO, we select the subset of 20 classes that overlap with the objects in EPIC-Kitchens, and use the provided bounding box annotations to create our classification dataset as before. For both datasets, we balance the test set to have an equal number of images per class, resulting in 1340 images (across 67 classes) in EPIC-Kitchens, and 5700 images (across 20 classes) in COCO for testing.

For the classifier, we adopt a two-stream model. The first stream transforms the 2048D feature from a pretrained ResNet-50 into a 1024D vector using a fully connected layer followed by ReLU. The second stream transforms the auxiliary features (from hotspot maps for example) by performing a 1x1 convolution followed by a ReLU on the input features to get a (256,7,7) feature. This is then flattened and transformed to a 1024D vector for classification similar to the first stream. Our autoencoder

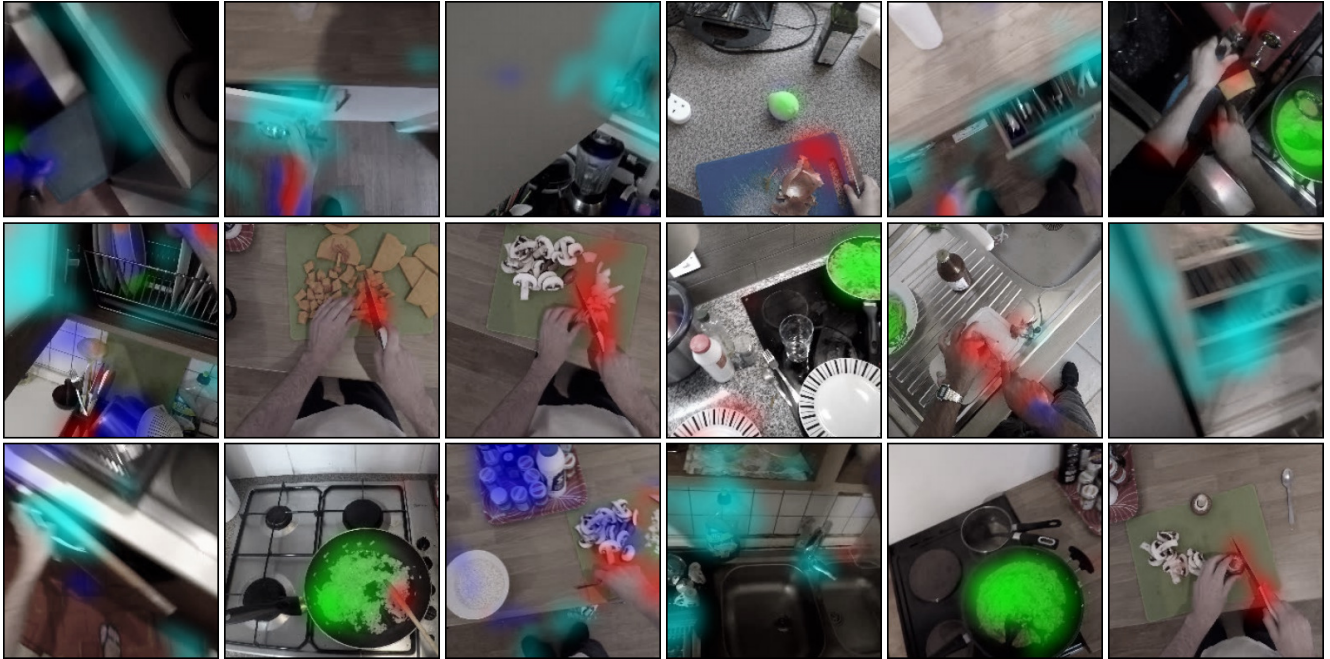


**Figure 7: Generated interaction hotspot maps on EPIC-Kitchens frames.** Our interaction hotspot maps show cuttable, mixable, holdable, and openable regions (in red, green, blue, and cyan, respectively).

baseline is a convolutional autoencoder with nearest-neighbor interpolation. It consists of 5 (conv-relu-bn) blocks in the encoder and decoder, with an encoded feature size of 2048.

### Additional Examples of Generated Hotspot Maps

We provide more examples of our hotspot maps to accompany our results in the main paper. Figure 6 contains more examples of these on the OPRA dataset to supplement our results in Figure 3 in the main paper. Unlike the baselines, our model highlights multiple distinct affordances for an object and does so without heatmap annotations during training. The last 4 images show some failure cases where our model is unable to produce heatmaps for small or unfamiliar objects.

Figure 7 and Figure 8 contain more examples of our hotspot maps on EPIC-Kitchens and COCO, equivalent to Figure 5 in the main paper, highlighting our model’s performance on more diverse and realistic data. Some failure modes of our models can be seen in the last 4 images in Figure 8. Inconsistencies in scale and viewpoint compared to the ego-centric video used for training, which results in diffused heatmaps over entire scenes (*e.g.* kitchens, bedrooms). Heatmaps for unfamiliar objects (*e.g.* people, cats) where the model defaults to producing heatmaps for dominant action classes like “open” as it is more frequently seen during training, thus learning stronger features.

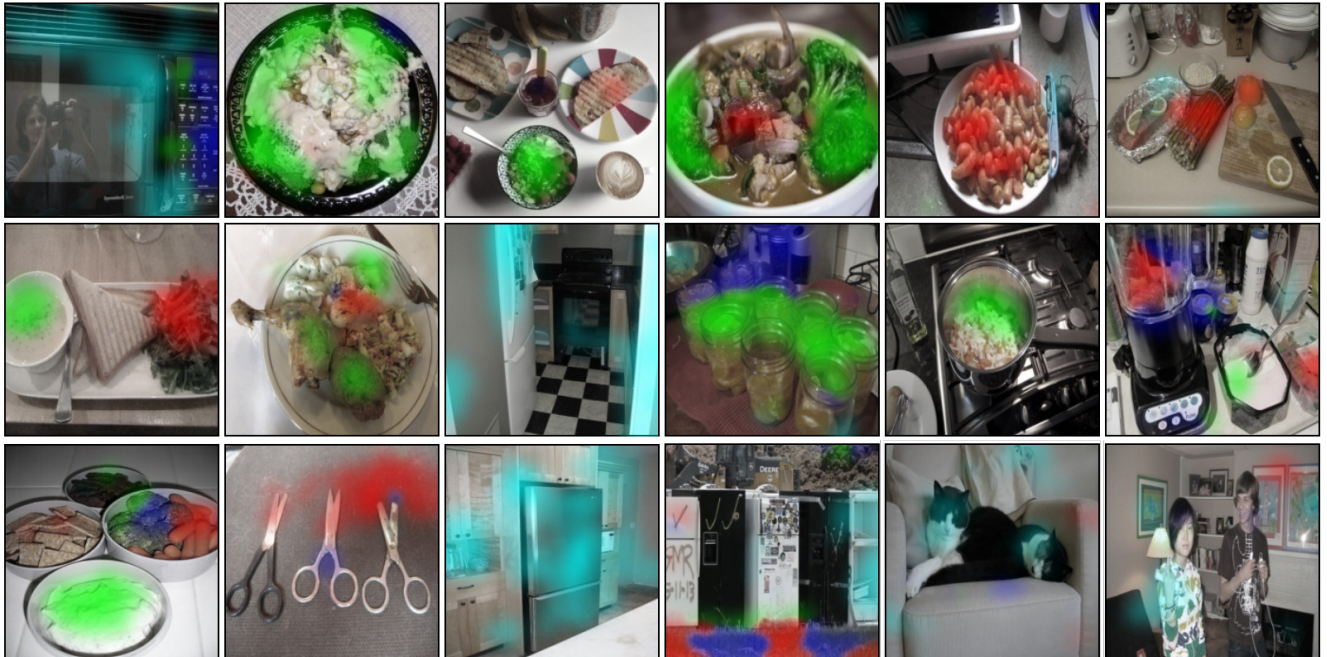


**Figure 8: Generated interaction hotspot maps on images from COCO.** Our interaction hotspot maps show cuttable, mixable, holdable, and openable regions (in red, green, blue, and cyan, respectively). Some failure cases due to unusual viewpoints and unfamiliar objects/actions can be seen in the last 4 examples.